Drastic enhancement of X-ray scattering contrast between amorphous and crystalline phases of poly(3-hexylthiophene) at the sulfur K-edge

Guillaume Freychet,[1] Yuxuan Huang,[2] Wen Liang Tan,[3] Peter A. Gilhooly-Finn,[4,5] Christian B. Nielsen,[4] Henning Sirringhaus,[2] and Christopher R. McNeill,[3,*]

[1] NSLS-II, Brookhaven National Laboratory, Upton, NY 11973, USA

[2] Cavendish Laboratory, University of Cambridge, J J Thomson Avenue, Cambridge CB3 0HE, United Kingdom

[3] Department of Materials Science and Engineering, Monash University, Wellington Road, Clayton, Victoria 3800, Australia.

[4] Department of Chemistry, Queen Mary University of London, Mile End Road, London E1 4NS, UK

[5] Department of Chemistry, University College London, 20 Gordon Street, London, WC1H 0AJ, UK

Poly(3-hexylthiophene), P3HT, SAXS, tender X-rays, sulfur.

ABSTRACT: Semicrystalline semiconducting polymers such as poly(3-hexylthiophene) exhibit hierarchical molecular ordering that influences their optoelectronic properties. As well as possessing crystalline order on the molecular scale, P3HT also exhibits regular ordering of crystalline lamellae on the nanoscale. This layering of crystalline and amorphous regions is characterized by the so-called "long period" which can be measured with small angle X-ray scattering (SAXS). The weak scattering contrast between amorphous and crystalline phases generally requires SAXS measurement of bulk powder samples. Here, we show that utilizing polarized tender X-rays tuned to the sulfur K-edge that strong contrast between amorphous and crystalline phases can be generated allowing the long period of thin film P3HT samples to be easily observed. Furthermore we show that the contrast generated results from differences in orientational order in the amorphous and crystalline regions. The use of resonant tender X-ray scattering is thus a promising technique for studying nanoscale ordering not only in semiconducting polymers but for other soft matter systems.

Semiconducting polymers derive their optoelectronic properties from alternating single and double bonds along their backbone.[1] Important semiconducting properties such as band-gap and charge carrier mobility are sensitive not only to the chemical structure of the repeat unit, but also to the precise polymer chain conformation and molecular packing.[2] Many semiconducting polymers are semicrystalline, with highly ordered crystalline regions surrounded by disordered amorphous regions.[3]

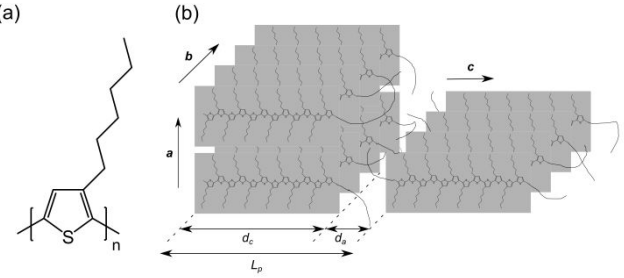

Figure 1. (a) Chemical structure of P3HT. (b) Schematic of the molecular packing of P3HT identifying the main crystallographic axes, *a*, *b*, *c*, along with the formation of crystalline lamellae of width d_c along the direction of the c axis which are separated by amorphous layers of thickness d_a. The long period L_p is then equal to $d_a + d_c$.

Poly(3-hexylthiophene) or P3HT is arguably the most important semiconducting polymer if not the most well-studied.[4] With a relatively high degree of crystallinity and reasonable charge carrier mobility, regioregular P3HT has been studied in a wide range of applications including organic field-effect transistors,[5] polymer solar cells[6] and polymer thermoelectrics.[7] P3HT crystals are characterized by sheets of π-stacked planar backbones separated by layers of insulating alkyl side chains, see Figure 1. While the alkyl side chains themselves are not electrically active, they play an important role in templating molecular packing and thus indirectly influence the resulting optoelectronic properties of the material. The most common crystal polymorph of P3HT ("Form I") has a monoclinic unit cell with *a* axis directed along the alkyl stacking direction, *b* axis directed along the π-π stacking direction and *c* axis directed along the polymer backbone.[8] Unit cell dimensions are ~ 17 Å along the alkyl stacking direction and ~ 7.8 Å along the π-π stacking and backbone stacking directions.[9, 10] This unit cell accommodates two chemical repeat units along the π-π stacking and backbone stacking directions (according to the $P2_1/c$ space group) giving a separation of neighboring polymer chains along the *b* axis of ~ 3.9 Å.[9]

Like other semicrystalline polymers, P3HT exhibits molecular ordering on the nanoscale, forming crystalline lamellae. By controlling the growth of P3HT crystals, micron long P3HT nanofibers can be produced with the fiber axis parallel to the π-π stacking direction.[11] The width of such lamellae along the polymer backbone direction is generally less than 20 nm, limited by chain folding which occurs once the contour length of the polymer reaches a certain size.[12, 13] The stacking of P3HT lamellae along the polymer backbone direction can be remarkably regular consisting of layers of crystalline material separated by amorphous material, see Figure 1. This periodicity – known as the "long period" – is sufficient to produce a well-defined scattering peak that is observable with small angle X-ray scattering (SAXS)[14] due to the difference in the electron density of amorphous and crystalline P3HT. Bulk powders samples are generally required to experimentally measure the long period as the scattering contrast between amorphous and crystalline regions is too weak to be observed in thin films, even when using grazing incidence SAXS.[15] However, as thin films are used in devices it is important to be able to fully characterize the microstructure of thin films whose structure can differ from bulk samples. In particular, it has been demonstrated that the long period of P3HT is important in templating an optimum nanoscale morphology for efficient polymer solar cells[15, 16] and can impact charge carrier mobility.[12] It is worth noting that characterization of nanoscale structure is important in many other soft matter systems including non-conjugated polymers, block copolymers, liquid crystals and even biological systems.[17]

SAXS measurements of the long period of P3HT to date have relied upon use of hard X-rays whose energy is far removed from elemental absorption edges.[12, 14, 15, 18, 19] Contrast thus derives from a subtle difference in the mass (and hence electron) density of crystalline P3HT compared to amorphous P3HT.[15] Tuning the X-ray energy close to an elemental absorption edge provides the opportunity to dramatically change the contrast between crystalline and amorphous phases.[20] While there is no chemical difference between amorphous P3HT and crystalline P3HT, polarization dependent effects can be exploited owing to the highly anisotropic properties of semiconducting polymer crystals. Indeed, we have recently reported strong anisotropic X-ray diffraction effects at the sulfur K-edge for the well-studied electron transporting semiconducting polymer P(NDI2OD-T2).[21, 22]

Figure 2a,b shows X-ray scattering patterns of an aligned thin film sample of P3HT (M_n = 49 kg/mol, $Đ$ = 1.5, regioregularity > 99%) taken near the sulfur K-edge. These measurements were acquired at the Soft Matter Interfaces (SMI) beamline (Beamline 12-ID) at the National Synchrotron Light Source II.[23] Samples of ~ 60 nm thickness were aligned by mechanical rubbing with annealing at 180 °C before being transferred to X-ray transparent silicon nitride membranes. Samples were then measured in transmission with the X-ray beam perpendicular to the plane of the sample, see Figure S1 for a diagram of the measurement geometry. These rubbed samples exhibited a high degree of alignment, with further details of sample preparation and characterization provided in the supporting information. For the data shown in Figure 2, the polarization of the X-ray beam is aligned parallel to the rubbing direction and hence the backbone of the aligned chains. Data for two X-ray energies are shown: 2445 eV which is just below the sulfur K-edge (non-resonant) and 2477.25 eV which is resonant with the 1s → (S–C)σ* transition whose transition dipole moment is oriented along the backbone.[22] At the non-resonant energy, only one peak is observed at $q \sim 0.37$ Å^{-1} along the direction perpendicular to the backbone axis. This peak is the (100) alkyl stacking peak corresponding to an alkyl stacking distance of 17.0 Å and is produced by "face-on" oriented chains. For the resonant energy, two peaks are observed: the alkyl stacking peak is again observed at $q \sim 0.37$ Å^{-1} along with a new peak at $q \sim 0.038$ Å^{-1} oriented along the direction parallel to the backbone axis. This peak at lower q is identified with the long period of P3HT and based on the peak position corresponds to a spacing of ~16 nm. Note that the 2D images in Figure 2 have the same scale bar. Changes in intensity of both the long period peak and (100) peak are seen with changing photon energy, with analysis of the resonant effects of the (100) peak to be discussed in a separate paper. There is also an increase in the background intensity due to X-ray fluorescence which provides a convenient means for measuring the near-edge X-ray absorption fine structure (NEXAFS) spectrum of the sample as described previously.[21] The highly anisotropic scattering pattern also confirms the high degree of alignment of this sample.

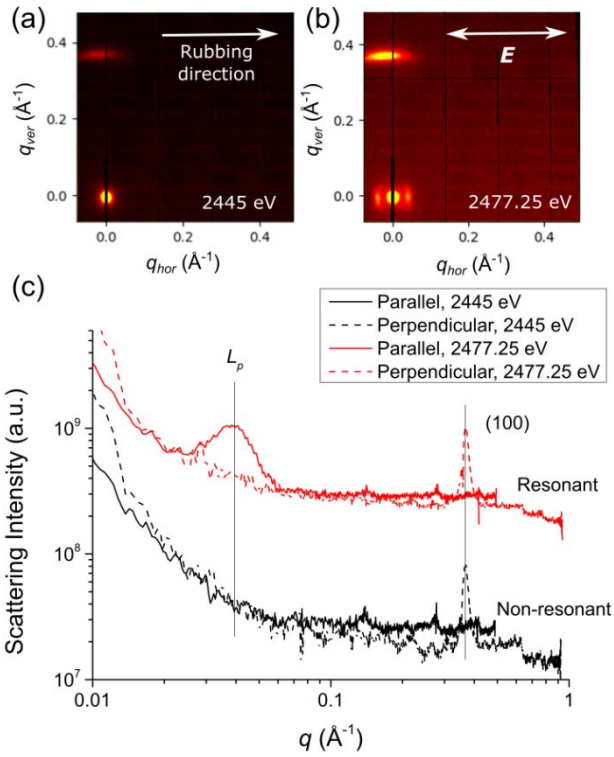

Figure 2. (a, b) Two-dimensional scattering patterns of a rubbed P3HT thin film taken at non-resonant, (a), and resonant, (b) X-ray energies. The rubbing direction and orientation of the electric field vector ***E*** of the polarized X-ray beam are also shown. The two images have the same intensity scale. (c) One-dimensional line profiles taken along directions parallel and perpendicular to the rubbing direction at non-resonant and resonant X-ray energies.

Figure 2c presents 1-dimensonal scattering profiles taken along directions parallel and perpendicular to the rubbing direction for the non-resonant and resonant energies. The long period peak at ~ 0.038 Å^{-1} is prominent in the scattering profile parallel to the rubbing direction at 2477.25 eV but not discernable at the non-resonant energy. The (100) peak is clearly seen in both resonant and non-resonant traces in the direction perpendicular to the rubbing direction but absent in the traces parallel to the rubbing direction. Using the resonant scattering profile it is possible to perform correlation function analysis to extract important microstructural information under the assumption of an ideal lamellar morphology.[24] This analysis is provided in the Supporting Information which returns a long period of L_p = 14.5 nm, average lamellar thickness of 5.6 nm and local crystallinity of 39%.

To better characterize the resonant behavior of the long period peak, scattering profiles were measured at various energies across the absorption edge from 2450 eV to 2500 eV. Peak fitting was performed for scattering profiles along the rubbing direction to extract the peak area of the long period peak. Peak parameters (location, width) were first determined for the energy with the largest peak area and then fixed for fitting of all other energies, with further details provided in the supporting information. Figure 3 presents a plot of peak area as a function of energy. A very sharp resonance is observed with fitted peak area increasing by a factor of over 80 from below the sulfur K-edge to a sharp peak at resonance at ~2477 eV. Indeed, the width (FWHM) of the resonant response is only 1.5 eV.

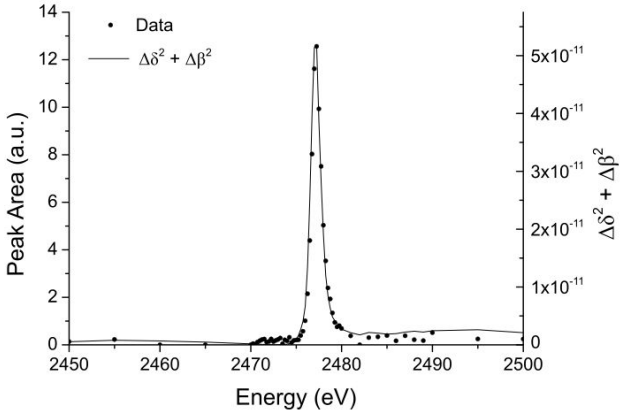

Figure 3. Plot of long period peak area as a function of photon energy (dots). Also shown for comparison is the contrast function $\Delta\delta^2 + \Delta\beta^2$ between amorphous and crystalline phases.

To explain this resonant behavior, we need to consider the energy-dependent anisotropic X-ray optical properties of P3HT. The energy dependent interaction between materials and X-rays can be described either in terms of energy dependent atomic scattering factors or in terms of an energy dependent refractive index. As scattering in this case results from differences in the properties of amorphous and crystalline regions, a refractive index treatment is adopted, although both approaches are equivalent and we have previously used energy-dependent atomic scattering factors to describe resonant X-ray diffraction of P(NDI2OD-T2).[21, 22] The complex index of refraction is then:

$$n = 1 - \delta - i\beta \quad (1)$$

where δ is the energy-dependent refraction decrement and β is the energy-dependent absorption index.[25] Far from absorption edges δ and β vary smoothly with X-ray energy. At an absorption edge, however, there are sharp changes in δ and β. For anisotropic materials, n will also depend upon the orientation of the polarization of the X-ray beam with respect to the sample, in this case with respect to the rubbing direction. For two materials with different n, or in this case for regions in the same material but with different n, the scattering contrast is given by:[25]

$$\text{Contrast} \sim \Delta\delta^2 + \Delta\beta^2 \quad (2)$$

where $\Delta\delta$ and $\Delta\beta$ are the energy dependent differences between δ and β of the two materials or the two regions. In the following we seek to derive the energy-dependent values for δ and β for the amorphous and crystalline regions of P3HT.

As the data in Figure 2 are for the case where the X-ray polarization is parallel to the rubbing direction, we seek values of δ and β corresponding to the X-ray polarization being parallel to the backbone in the crystalline regions of the lamellae. As β relates to the energy dependent absorption index it can be determined directly from X-ray absorption measurement with δ then determined via the Kramers-Kronig transformation. Figure 4a presents the fluorescence NEXAFS spectra of the rubbed P3HT sample taken with the X-ray polarization either parallel or perpendicular to the rubbing direction. Strong dichroism is observed, with the peak at 2477 eV strongest when the X-ray polarization is aligned with the rubbing direction and hence the backbone of aligned chains. This peak at 2477 eV is attributed to the 1s $\rightarrow$ (S–C)σ* transition with transition dipole moment is oriented along the backbone,[22] and is more intense than other resonant transitions. The spectrum taken with X-ray polarization parallel to the rubbing direction will closely resemble the NEXAFS spectrum of crystallites with polarization parallel to the c axis (backbone direction). However as this spectrum is likely to contain a contribution due to amorphous chains and/or unaligned chains, it was extrapolated using a difference spectrum as described in the Supporting Information. Figure 4b then presents the corrected spectra corresponding to the electric field vector, ***E***, of the X-ray beam being parallel and perpendicular to the backbone. The spectrum with ***E*** parallel to the backbone can be then taken as representative of aligned backbones in the crystalline regions of the lamellae. This spectrum can be converted to β by scaling the pre- and post-edge regions of the spectrum to the known photoabsorption cross sections of the constituent atoms and performing the necessary conversions to yield β.[25] This conversion was performed using KKCalc[26] which was also used to perform the Kramers-Kronig transformation to yield δ. The resulting values of δ and β for the crystalline regions with X-ray polarization oriented parallel to the backbone are shown in Figure 4c,d.

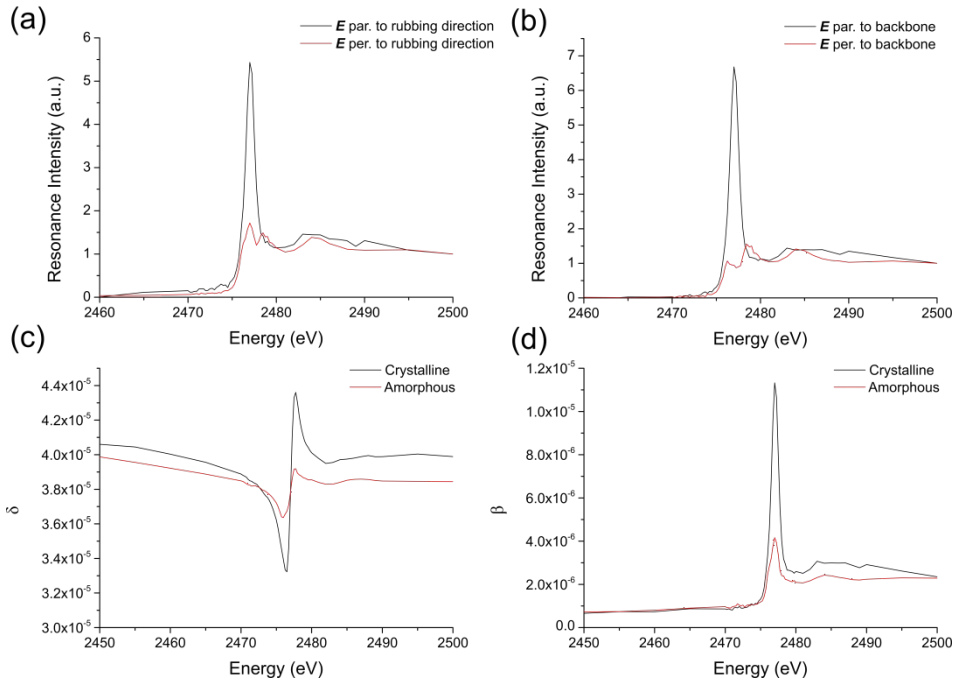

Figure 4. (a) Fluorescence NEXAFS spectra of the rubbed sample taken with polarization parallel and perpendicular to the rubbing direction. (b) Extrapolated spectra corresponding to polarization parallel and perpendicular to the backbone. (c,d) Plots of β, (c), and δ, (d), determined for the crystalline (with ***E*** parallel to the backbone) and amorphous regions. A density of 1.11 g/cm^3 was used for the amorphous regions while a density of 1.14 g/cm^3 was used for the crystalline regions.

For the amorphous regions it is assumed that there is no preferential orientation of chains with respect to X-ray polarization, and so n should be the same regardless of sample orientation. To derive values of δ and β for the amorphous regions, a NEXAFS spectrum taken of a spin-coated sample was used. Spin-coating results in no preferred in-plane orientation of polymer backbones meaning that the measured NEXAFS spectra are independent of azimuthal orientation of the X-ray polarization with respect to the sample. As P3HT samples can exhibit edge-on texture, a spectrum taken with polar angle close the so-called "magic angle" was used. The values of δ and β derived for the amorphous regions are also shown in Figure 4b,c. Note that the density of the material enters into the calculation of δ and β, with values of $\rho_{amor.}$ = 1.11 g/cm^3 and $\rho_{cryst.}$ = 1.14 g/cm^3 used which accounts for the differences in δ and β pre- and post-edge. A value of 1.14 g/cm^3 for the crystalline region was derived from the unit cell proposed by Kayunkid et al.[9] while the value for the amorphous fraction was taken based comparing the calculated contrast function with the observed resonant response as described below. Further details can be found in the Supporting Information.

The resulting contrast function, $\Delta\delta^2 + \Delta\beta^2$, is plotted in Figure 3 and compared to the observed resonant behavior of the long period peak. Excellent agreement is found between the calculated and observed resonant scattering behavior. In particular the calculated contrast function accurately describes the shape of the profile along with the relative enhancement in scattering intensity. It is noted that the calculated contrast function is sensitive to the density values used, with Figure S7 plotting $\Delta\delta^2 + \Delta\beta^2$ for different values of $\rho_{amor.}$.

We note that achieving a high scattering contrast between amorphous and crystalline phases relies upon exploiting the anisotropic optical properties of the crystalline phases. When the sample is rotated such that the polarization is perpendicular to the rubbing direction the long period peak is not observed even at resonance due there being insufficient differences between δ and β in that case (see Figure S8).

In summary, we have shown that differences in the local (anisotropic) refractive index near the sulfur K-edge for amorphous and crystalline regions can be exploited to enhance the scattering contrast between amorphous and crystalline phases in P3HT. This enhanced scattering contrast enables scattering from the long period in P3HT to be observed in thin film films using a transmission geometry. This advance provides a new avenue to study nano and mesoscale ordering in thin films of sulfur-containing semiconducting polymers that are important for device function. Furthermore, the approach presented for enhancing contrast between amorphous and crystalline phases is likely to be of benefit to other fields of soft condensed matter.

ASSOCIATED CONTENT

Supporting Information. Extra details of sample preparation and measurement; details of peak fitting; further details regarding determination of δ and β; scattering data taken with sample oriented with rubbing direction perpendicular to beam polarization. This material is available free of charge via the Internet at http://pubs.acs.org.

AUTHOR INFORMATION

Corresponding Author

* Christopher R. McNeill –Department of Materials Science and Engineering, Monash University, Clayton, Victoria 3800, Australia; orcid.org/0000-0001-5221-878X;
Email: christopher.mcneill@monash.edu

ACKNOWLEDGMENT

This research used the Soft Matter Interfaces (SMI) beamline (Beamline 12-ID) of the National Synchrotron Light Source II, a U.S. Department of Energy (DOE) Office of Science User Facility operated for the DOE Office of Science by Brookhaven National Laboratory under Contract DE-SC0012704. HS acknowledges financial support from the European Research Council for a Synergy grant SC2 (no. 610115) and from the Engineering and Physical Sciences Research Council (EP/R031894/1). The authors thanks Mikhail Zhernenkov (NSLS-II) for his assistance at the beamline and for the helpful discussions.

REFERENCES

1. Heeger, A. J., Semiconducting polymers: the Third Generation. *Chem. Soc. Rev.* **2010,** 39, 2354-2371.

2. Olivier, Y.; Niedzialek, D.; Lemaur, V.; Pisula, W.; Müllen, K.; Koldemir, U.; Reynolds, J. R.; Lazzaroni, R.; Cornil, J.; Beljonne, D., 25th Anniversary Article: High-Mobility Hole and Electron Transport Conjugated Polymers: How Structure Defines Function. *Adv. Mater.* **2014,** 26, 2119-2136.

3. Salleo, A.; Kline, R. J.; DeLongchamp, D. M.; Chabinyc, M. L., Microstructural Characterization and Charge Transport in Thin Films of Conjugated Polymers. *Adv. Mater.* **2010,** 22, 3812-3838.

4. Ludwigs, S., *P3HT Revisited – From Molecular Scale to Solar Cell Devices*. Springer: 2014; Vol. 265.

5. Sirringhaus, H.; Brown, P. J.; Friend, R. H.; Nielsen, M. M.; Bechgaard, K.; Langeveld-Voss, B. M. W.; Spiering, A. J. H.; Janssen, R. A. J.; Meijer, E. W.; Herwig, P.; de Leeuw, D. M., Two-dimensional charge transport in self-organized, high-mobility conjugated polymers. *Nature* **1999,** 401, 685-688.

6. Dang, M. T.; Hirsch, L.; Wantz, G., P3HT:PCBM, Best Seller in Polymer Photovoltaic Research. *Adv. Mater.* **2011,** 23, 3597-3602.

7. Lim, E.; Glaudell, A. M.; Miller, R.; Chabinyc, M. L., The Role of Ordering on the Thermoelectric Properties of Blends of Regioregular and Regiorandom Poly(3-hexylthiophene). *Adv. Electron. Mater.* **2019,** 5, 1800915.

8. Brinkmann, M., Insights into the structural complexity of semi-crystalline polymer semiconductors: electron diffraction contributions. *Mater. Chem. Front.* **2020,** 4, 1916-1929.

9. Kayunkid, N.; Uttiya, S.; Brinkmann, M., Structural Model of Regioregular Poly(3-hexylthiophene) Obtained by Electron Diffraction Analysis. *Macromolecules* **2010,** 43, 4961-4967.

10. Dudenko, D.; Kiersnowski, A.; Shu, J.; Pisula, W.; Sebastiani, D.; Spiess, H. W.; Hansen, M. R., A Strategy for Revealing the Packing in Semicrystalline π-Conjugated Polymers: Crystal Structure of Bulk Poly-3-hexyl-thiophene (P3HT). *Angew. Chem. Int. Ed.* **2012,** 51, 11068-11072.

11. Persson, N. E.; Chu, P.-H.; McBride, M.; Grover, M.; Reichmanis, E., Nucleation, Growth, and Alignment of Poly(3-hexylthiophene) Nanofibers for High-Performance OFETs. *Acc. Chem. Res.* **2017,** 50, 932-942.

12. Singh, C. R.; Gupta, G.; Lohwasser, R.; Engmann, S.; Balko, J.; Thelakkat, M.; Thurn-Albrecht, T.; Hoppe, H., Correlation of charge transport with structural order in highly ordered melt-crystallized poly(3-hexylthiophene) thin films. *J. Polym. Sci. Part B: Polym. Phys.* **2013,** 51, 943-951.

13. Brinkmann, M.; Rannou, P., Molecular Weight Dependence of Chain Packing and Semicrystalline Structure in Oriented Films of Regioregular Poly(3-hexylthiophene) Revealed by High-Resolution Transmission Electron Microscopy. *Macromolecules* **2009,** 42, 1125-1130.

14. Kohn, P.; Huettner, S.; Komber, H.; Senkovskyy, V.; Tkachov, R.; Kiriy, A.; Friend, R. H.; Steiner, U.; Huck, W. T. S.; Sommer, J.-U.; Sommer, M., On the Role of Single Regiodefects and Polydispersity in Regioregular Poly(3-hexylthiophene): Defect Distribution, Synthesis of Defect-Free Chains, and a Simple Model for the Determination of Crystallinity. *J. Am. Chem. Soc.* **2012,** 134, 4790-4805.

15. Kohn, P.; Rong, Z.; Scherer, K. H.; Sepe, A.; Sommer, M.; Müller-Buschbaum, P.; Friend, R. H.; Steiner, U.; Hüttner, S., Crystallization-Induced 10-nm Structure Formation in P3HT/PCBM Blends. *Macromolecules* **2013,** 46, 4002-4013.

16. Sepe, A.; Rong, Z.; Sommer, M.; Vaynzof, Y.; Sheng, X.; Mueller-Buschbaum, P.; Smilgies, D.; Tan, Z.-K.; Yang, L.; Friend, R.; Steiner, U.; Huttner, S., Structure Formation in P3HT/F8TBT Blends. *Energy & Environ. Sci.* **2014,** 7, 1725-1736.

17. Collins, B. A.; Gann, E., Resonant soft X-ray scattering in polymer science. *J. Polym. Sci.* **2022,** in press, https://doi.org/10.1002/pol.20210414.

18. Wu, Z.; Petzold, A.; Henze, T.; Thurn-Albrecht, T.; Lohwasser, R. H.; Sommer, M.; Thelakkat, M., Temperature and Molecular Weight Dependent Hierarchical Equilibrium Structures in Semiconducting Poly(3-hexylthiophene). *Macromolecules* **2010,** 43, 4646-4653.

19. Kohn, P.; Huettner, S.; Steiner, U.; Sommer, M.,

Fractionated Crystallization of Defect-Free Poly(3-hexylthiophene). *ACS Macro Lett.* **2012,** 1, 1170-1175.

20. Hodeau, J.-L.; Favre-Nicolin, V.; Bos, S.; Renevier, H.; Lorenzo, E.; Berar, J.-F., Resonant Diffraction. *Chem. Rev.* **2001,** 101, 1843-1868.

21. Freychet, G.; Gann, E.; Thomsen, L.; Jiao, X.; McNeill, C. R., Resonant Tender X-ray Diffraction for Disclosing the Molecular Packing of Paracrystalline Conjugated Polymer Films. *J. Am. Chem. Soc.* **2021,** 143, 1409-1415.

22. Freychet, G.; Gann, E.; Zhernenkov, M.; McNeill, C. R., Anisotropic Resonant X-ray Diffraction of a Conjugated Polymer at the Sulfur K-edge. *J. Chem. Phys. Lett.* **2021,** 12, 3762-3766.

23. Zhernenkov, M.; Canestrari, N.; Chubar, O.; DiMasi, E., Soft matter interfaces beamline at NSLS-II: geometrical ray-tracing vs. wavefront propagation simulations. *Proc. SPIE* **2014,** 9209, 92090G.

24. Strobl, G. R.; Schneider, M., Direct evaluation of the electron density correlation function of partially crystalline polymers. *J. Polym. Sci. Polym. Phys. Ed.* **1980,** 18, 1343-1359.

25. Ade, H.; Hitchcock, A., NEXAFS microscopy and resonant scattering: composition and orientation probed in real and reciprocal space. *Polymer* **2008,** 49, 643-675.

26. Watts, B., Calculation of the Kramers-Kronig transform of X-ray spectra by a piecewise Laurent polynomial method *Opt. Express* **2014,** 22, 23628-23639.

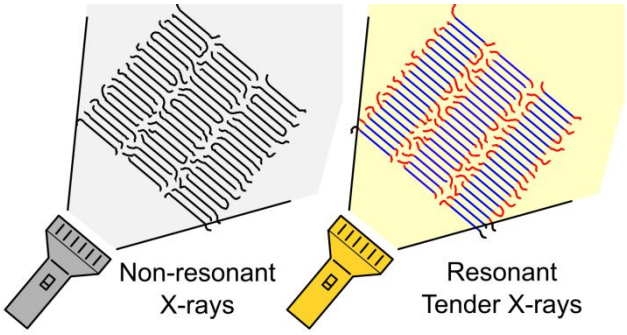
Non-resonant
X-rays
Resonant
Tender X-rays